

RESEARCH ARTICLE

The initiation and early development of apical—basal polarity in Toxoplasma gondii

Luisa F. Arias Padilla*, Jonathan Munera Lopez*, Aika Shibata, John M. Murray and Ke Hu[‡]

ABSTRACT

The body plan of the human parasite Toxoplasma gondii has a well-defined polarity. The minus ends of the 22 cortical microtubules are anchored to the apical polar ring, which is a putative microtubuleorganizing center. The basal complex caps and constricts the parasite posterior end and is crucial for cytokinesis. How this apical-basal polarity is initiated is unknown. Here, we have examined the development of the apical polar ring and the basal complex using expansion microscopy. We found that substructures in the apical polar ring have different sensitivities to perturbations. In addition, apicalbasal differentiation is already established upon nucleation of the cortical microtubule array: arc forms of the apical polar ring and basal complex associate with opposite ends of the microtubules. As the nascent daughter framework grows towards the centrioles, the apical and basal arcs co-develop ahead of the microtubule array. Finally, two apical polar ring components, APR2 and KinesinA, act synergistically. The removal of individual proteins has a modest impact on the lytic cycle. However, the loss of both proteins results in abnormalities in the microtubule array and in highly reduced plaquing and invasion efficiency.

KEY WORDS: Cell polarity, Organizing center, Apical polar ring, Basal complex, Microtubule, Toxoplasma

INTRODUCTION

The ~6000 known members of the phylum Apicomplexa are unicellular parasites that infect a wide range of invertebrate and vertebrate hosts (Seeber and Steinfelder, 2016). Many of them cause devastating diseases in humans, such as cryptosporidiosis, toxoplasmosis and malaria (Torgerson and Mastroiacovo, 2013; Checkley et al., 2015; Seeber and Steinfelder, 2016; World Health Organization World Malaria Report 2022, https://www.who.int/ teams/global-malaria-programme/reports/world-malaria-report-2022). The apicomplexans are also excellent models for exploring the construction, function and evolution of cellular architectures, due to their sophisticated membrane and cytoskeletal structures, and to the de novo generation of a membrane-cytoskeletal scaffold for daughter cells during cell division (Hepler et al., 1966; Sheffield and Melton, 1968; Sheffield, 1970; Dubremetz and Elsner, 1979; Hu et al., 2002a; Morrissette and Sibley, 2002; Voß et al., 2023) (Fig. 1).

Biodesign Center for Mechanisms of Evolution, School of Life Sciences, Arizona State University, Tempe, AZ 85281, USA

[‡]Author for correspondence (kehu4@asu.edu)

() K.H., 0000-0001-9778-7337

Handling Editor: Michael Way Received 15 July 2024; Accepted 2 September 2024

In Toxoplasma gondii, the cellular organization has been best studied in the tachyzoite form of the parasite, which is responsible for acute toxoplasmosis via invasion of host cells by gliding motility, rapid intracellular replication and subsequent active egress that destroys the host cell (Frenkel, 1973; Lyons et al., 2002; Morrissette and Sibley, 2002). The two poles of the parasite are marked by the apical and basal complexes, respectively (Nichols and Chiappino, 1987; Hu et al., 2006; Hu, 2008) (Fig. 1). The cytoskeletal elements of the apical complex include the apical polar ring, the conoid and associated preconoidal rings, and the two intraconoid microtubules (MTs) (Nichols and Chiappino, 1987; Morrissette et al., 1997; Hu et al., 2002b). The conoid is formed of highly curved, ribbon-like tubulin fibers (Hu et al., 2002b; Sun et al., 2022; Gui et al., 2023; Li et al., 2023). The entire conoid protrudes or retracts through the apical polar ring in a Ca²⁺dependent manner. The apical polar ring is also structurally integrated with the minus ends of the 22 cortical MTs in mature parasites (Russell and Burns, 1984; Hu et al., 2002b; Wang et al., 2021; Sun et al., 2022; Li et al., 2023). The removal of two apical polar ring components (KinesinA and APR1) results in MT detachment from the apex in mature parasites (Leung et al., 2017). However, it is unknown how this putative MT-organizing center is assembled and how it develops with respect to the MT array.

The basal complex caps and constricts the posterior end of the parasite (Gubbels et al., 2006; Hu et al., 2006; Hu, 2008; Heaslip et al., 2010; Lorestani et al., 2010). Although the sophistication of the apical complex is immediately obvious from its striking structure and has been known for many decades, the complexity of the basal complex was not recognized until much later, when multiple components of the basal complex were identified in a proteomic screen (Hu et al., 2006). That screen was designed to identify components of the apical complex, but unexpectedly a number of the apical complex components were also localized to the basal complex. One of them, MORN1, is weakly localized to the apical complex, but has a very prominent localization to the basal complex and the spindle pole. Later, MORN1 was found to be important for maintaining the constriction of the parasite posterior end and for successful cytokinesis (Heaslip et al., 2010; Lorestani et al., 2010). In daughter parasites, the basal complex was first observed as a ring abutting the distal end of the cortical MTs (Hu et al., 2006; Hu, 2008). After the daughters emerge from the mother parasite, the basal complex disengages from the cortical MTs via an unknown mechanism and becomes the basal cap of the mature parasite. Although MORN1 and some other components of the basal complex have been shown to be recruited to early daughters (Hu, 2008; Engelberg et al., 2022), how the basal complex initiates and develops into a ring was not known due to the limited temporal and spatial resolution of existing microscopy data.

Recently, we investigated the initiation and early development of the tubulin-containing structures in Toxoplasma using expansion microscopy (ExM) (Padilla et al., 2024). We discovered that the 22

^{*}These authors contributed equally to this work

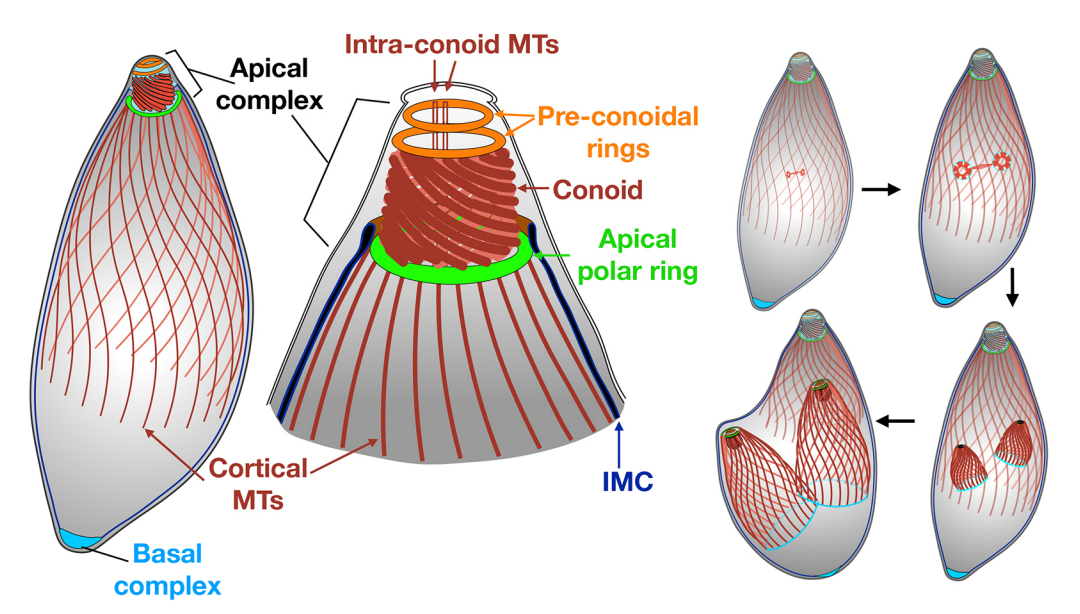


Fig. 1. Schematic of tubulincontaining and -associated structures (left), and daughter formation throughout the cell cycle (right). For clarity, the cortical MTs of the mother are shown in a lighter color. IMC, inner membrane complex. Other membrane-bound organelles are not shown.

cortical MTs are not initiated at the same time. The daughter MT arrays are first detected close to the duplicated centrioles as incomplete cogwheels, in which six or seven 'stubs' of MTs form around the primordial conoid. The assembly of the MT array proceeds towards the centrioles. With the elongation and addition of more MTs, 'petals' that contain four or six MTs form in the disc-like nascent daughters. After all 22 MTs are nucleated, the five-fold symmetry of the early MT array becomes established, often with a 4, 4, 4 and 6 grouping pattern. This study uncovered distinct structural intermediates during nucleation, elongation and symmetry development of the array. It also raised the question of how the cytoskeletal complexes that associate with the opposite ends of the MT array develop, that is, do they follow a concerted or disjoint assembly path with respect to each other and to the MT array?

Here, we address these questions by delineating the localization of components of the apical polar ring (APR2) and the basal complex (MORN1) in intracellular *Toxoplasma* tachyzoites using ExM. The results reveal the extremely early establishment of the apical–basal polarity and a striking co-development of the arc-form precursors of the apical polar ring and the basal complex at opposite ends of the cortical MTs. We also found that different structural domains in the apical polar ring have different sensitivities to perturbations. Finally, we examined the impact of loss of APR2 alone and with KinesinA, and found that these two proteins act synergistically in plaquing efficiency, MT organization and parasite invasion.

RESULTS

The apical polar ring develops ahead of the cortical MT array during the initial assembly of the array

Previously, we carried out a comparative proteomic screen to identify protein components of the apical complex of Toxoplasma (Hu et al., 2006). For one of the proteins, TgGT1_227000, 10 peptides and 16 spectra were captured in the apical complex-enriched fraction and no peptides were found in the apical complex-depleted fraction. TgGT1_227000 contains segments that show weak similarity with the Atrophin-1 [N-terminal ~375 amino acids (aa)] and SMC_prok_B domain (~C-terminal ~550 aa). It is well-conserved within Conoidasida ($E_{Eimeria\ tenella}=9\times10^{-43}$). More distant homologs are also found in $Plasmodium\ spp.\ (E_{Plasmodium\ vivax}=2\times10^{-15})$. Confirming the highly significant enrichment in the apical

complex-fraction in our work, TgGT1_227000 has also been identified as one of the apical complex proteins in a more recent BioID screen (Koreny et al., 2021). In that study, TgGT1_227000 was localized to the apical polar ring of the mature parasites, but its localization in the daughter parasites was not determined.

To investigate the localization of this protein during daughter development, we generated a knock-in parasite line in which TgGT1_227000 (now named as the apical polar ring protein 2 or APR2) is endogenously tagged with mEmerald. In this line, the genomic locus of APR2 is replaced with a LoxP-flanked DNA fragment that contains the coding sequence (CDS) of mEmerald-APR2 with a 3' untranslated region (UTR) and a selectable marker cassette (Fig. 2A). Three-dimensional structured illumination microscopy (3D-SIM) confirmed the localization to the apical polar ring in mature parasites (Fig. 2B, arrowheads). Additionally, APR2 is detected at the apex of nascent daughters, before the dome-like shape of the daughters can be discerned (Fig. 2B, white arrows). This provides an opportunity to answer crucial questions related to the spatial and temporal relationship between the development of the apical polar ring and the cortical MT array: does the apical polar ring assemble into a ring before nucleation of the MTs or does it co-develop with the MT array?

The resolution of 3D-SIM imaging is insufficient to resolve the detailed structures of the apical polar ring and the MT array. We therefore examined the assembly of the apical polar ring and the MT array using ExM. The mEmeraldFP-APR2 (mE-APR2) knock-in parasite was labeled with an anti-GFP and an anti-tubulin antibody. Using the number and length of cortical MTs as the reference, we constructed an image sequence that reveals a distinct pattern of co-development of the apical polar ring and the MT array (Fig. 3A-K). We found that the assembly of the apical polar ring is initiated before that of the MT array. The precursor of the ring is first detected as an arc in the vicinity of the centrioles before the MT array is detectable (Fig. 3A). After the daughter tubulin-cytoskeleton appears, the APR2 arc fits between the primordial conoid and the MT array. Similar to the incomplete MT array, the opening of this arc consistently faces the centriole region, suggesting a biased growth direction towards the centrioles. Interestingly, the arc of the APR2 labeling often extends beyond the forming MT array towards the centrioles (arrowheads, Fig. 3A–G, K). The apical polar ring takes on

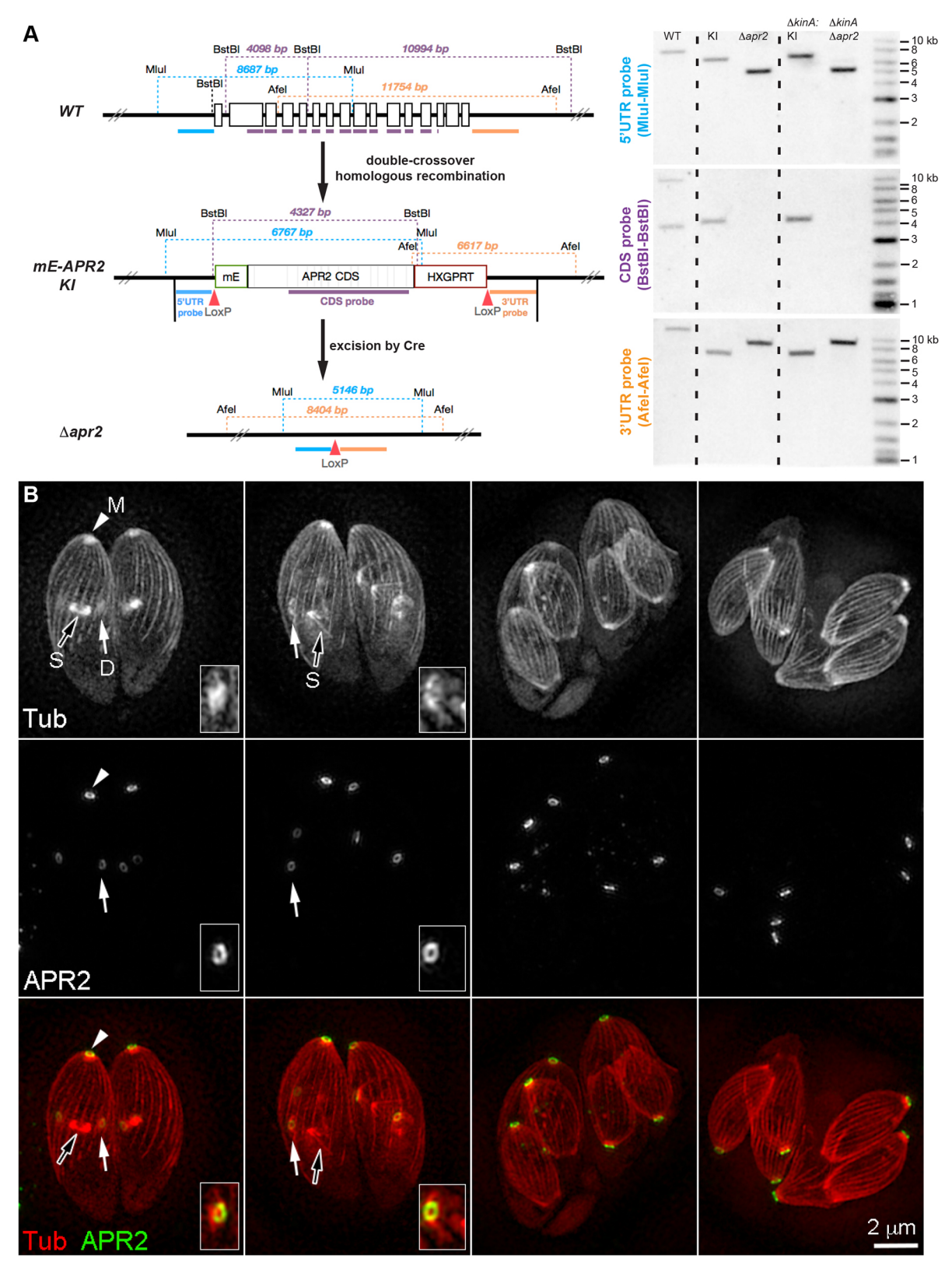


Fig. 2. See next page for legend.

its final ring-like shape before the completion of the nucleation of all 22 cortical MTs (Fig. 3G-I). This, for the first time, reveals how the growth of the apical polar ring might direct that of the MT array. It is conceivable that the leading extension of the apical polar ring guides

the initiation of new MTs by laying down or recruiting new nucleation complexes. Together, the development of both the apical polar ring and the MT array reveals a clear temporal gradient. MTs closer to the centriole region are younger; that is, constructed later.

Fig. 2. Generation of mEmeraldFP-APR2 knock-in and ∆apr2 parasites, and localization of APR2 in live parasites. (A) Left: schematic for generating the mEmeraldFP-APR2 knock-in (mE-APR2 KI) and ∆apr2 parasites, and Southern blotting strategy. Restriction sites, hybridization sections of the Southern blot probes for the apr2-coding region (CDS, purple bars), regions upstream ('5' UTR probe', blue bars) and downstream ('3' UTR probe', orange bars) of the CDS, and the corresponding DNA fragment sizes expected are indicated. Vertical black bars in the mE-APR2 KI schematic indicate the boundary of the sequences of 5' and 3'UTR included in the pTKO2_II-mE-APR2 knock-in plasmid used for generating the *mE-APR2* KI parasite. Right: Southern blots of the RH∆ku80 parental (WT), mE-APR2 knock-in (KI), Δapr2, ΔkinesinA: mE-APR2 knock-in (ΔkinA: KI) and $\Delta kinesinA\Delta apr2$ ($\Delta kinA\Delta apr2$) parasites. The hybridization patterns confirmed the homologous integration of the mE-APR2 fusion in the KI and $\Delta kinesinA$:KI parasites, and the deletion of the apr2 locus in the $\Delta apr2$ and ∆kinesinA∆apr2 parasites. The expected patterns are described in the Materials and Methods. A total of three Southern blot experiments were carried out for WT. KI and Appr2 parasites, two for the AkinesinA:KI parasites, and one for two independent clones of the ∆kinA∆apr2 parasites. (B) Projections of 3D-SIM images of live mE-APR2 knock-in Toxoplasma parasites expressing mAppleFP-β-tubulin1, in which cortical MTs are fluorescently labeled. mE-APR2 is detected in nascent daughters forming close to the centrioles (first and second columns). Image contrast was adjusted to optimize display. White arrows indicate daughter (D) structures (shown at twice the magnification in the insets). Arrowheads indicate the mother apical complex (M). Black arrows indicate the spindle (S). Images in the figure were selected as most clearly representing the relevant features, chosen from 3D stacks of 99 parasites in two experiments.

The basal complex develops in concert with the apical polar ring

We discovered previously that markers for both the apical structures and the basal complex are recruited to early daughters (Hu et al., 2006; Hu, 2008). The earliest discernible basal complex structure takes the form of a ring, which first expands, then constricts, and eventually forms a basal capping structure in the mature parasite (Hu, 2008). However, how the apical-basal axis in nascent daughters is established during MT development was not known. Also unknown was the path that the basal complex follows to form into a ring. To address this, we examined the assembly of the basal complex with respect to that of the apical polar ring and the tubulin-containing structures using ExM. We and others have previously discovered that MORN1 is one of the major components of the basal complex (Gubbels et al., 2006; Hu et al., 2006; Hu, 2008; Heaslip et al., 2010; Lorestani et al., 2010). Using a MORN1 antibody, we labeled the basal complex at various stages of daughter formation (Fig. 4A-J; Fig. S1). We found that the apical complex (including the conoid and the apical polar ring), the cortical MTs and the basal complex develop in concert. In the earliest detectable daughters, where only six or seven stubs of newly nucleated cortical MTs are present, the primordial basal complex is assembled as an arc at the outer circumference of the MT array, while at the same time the arc of the primordial apical polar ring is assembled at the inner circumference of the array (Fig. 4A). Before closing into a ring, the opening of the basal arc remains facing the centriole, in the same way as the MT array and the conoid (Fig. 4A-D). As the cortical MTs grow in length, the distance between the apical and basal arcs increases. While the radius of the apical polar arc/ring remains nearly constant throughout the assembly process, that of the basal complex increases as the MTs grow outwards (Fig. 4A-H). The arc form of the basal complex in early daughters was also recently reported by Engelberg et al. (2024) preprint) when this article was in preparation. Similar to the apical polar ring, the extension of the basal complex leads that of the MT array (Fig. 4A-E, arrowheads). The closure of the MORN1 ring occurs before all 22 MTs are nucleated (Fig. 4E). This suggests that

the development of the basal complex is likely independent of that of the MT array, even though the assembly of these two sets of structures is highly coordinated. Of note, when ectopically expressed in bacteria, MORN1 can form ring-like structures, indicating that it has an intrinsic ring-forming propensity (Heaslip et al., 2010). It is therefore conceivable that the basal ring formation is at least partly self-driven by core components such as MORN1, but the localization, timing and direction of assembly might be modulated by proteins that couple the basal complex to the MT array.

Previously, we generated a triple knockout mutant (denoted TKO) in which three MT associated proteins, TLAP2, TLAP3 and SPM1, were removed (Liu et al., 2015). The cortical MTs are destabilized in mature TKO parasites. The destabilization is particularly exacerbated in dividing parasites (Tengganu et al., 2023). Here, we found that the development of the daughter apical polar ring, and the basal complex are not affected in the TKO parasite (Fig. 5A,B). Often only a collar of tubulin surrounding the apical polar ring is left at the apex of the mother parasite (Fig. 5B, insets), which results in a striking, exposed view of the daughter frameworks in the full projection of the parasite.

The apical polar ring contains distinct substructures with different sensitivities to perturbations

Previously, we identified another early component of the apical polar ring, KinesinA (Leung et al., 2017). To determine the interdependency of early components of the apical polar ring, we generated a $\Delta kinesinA$: mE-APR2 knock-in line, and found that APR2 remains associated with the apical polar ring in the absence of KinesinA (Fig. 6A). Therefore APR2 localization is independent of that of KinesinA. When KinesinA was knocked out together with APR1, a later component of the apical polar ring, the cortical MTs detached from the apex in mature parasites (Leung et al., 2017). The labeling of RNG1, another apical polar ring component (Tran et al., 2010), also fragments in the $\Delta kinesinA\Delta apr I$ parasites. To determine whether APR2 localization is affected the same way, we generated a $\Delta kinesinA\Delta apr1: mE-APR2$ knock-in line and found that mE-APR2 labeling remains as a ring in the $\Delta kinesinA\Delta apr1$ parasite even when the MT dispersal from the apex is evident (Fig. 6B). To directly compare the RNG1 and APR2 localization, we generated RNG1mCherry expressing lines in both the wild-type and $\Delta kinesinA\Delta apr 1$: mE-APR2 knock-in background. We found that, in the wild-type parasite, APR2 and RNG1 labelings are distinct, with the RNG1 ring being wider and more basal. In the $\Delta kinesinA\Delta apr1$ parasite, the RNG1 labeling is fragmented (no longer an intact ring), whereas the ring of APR2 remains intact (Fig. 6C). This indicates that APR2 and RNG1 belong to two distinct structural domains that have different sensitivities to stress imposed on the apical polar ring during parasite growth.

Loss of APR2 alone does not have a detectable impact on the patterning of the cortical MTs or parasite lytic cycle, but the loss of both APR2 and KinesinA has a synergistic effect

To determine the structural impact of APR2 on the apical polar ring and MT organization, we generated an APR2 knockout line ($\Delta apr2$) by transiently expressing Cre recombinase in the mE-APR2 knockin parasite to excise the LoxP-mE-APR2-[selectable marker] cassette, generating individual clones that had lost the mE-APR2 fluorescence. We confirmed the excision of the APR2 locus by Southern blotting using probes specific to the APR2 CDS, as well as noncoding regions upstream (5') and downstream (3') from the CDS (Fig. 2A). To determine how combined loss of APR2 and KinesinA affects the patterning and development of the cortical MT array, we also generated $\Delta kinesinA\Delta apr2$ parasites from the $\Delta kinesinA$:

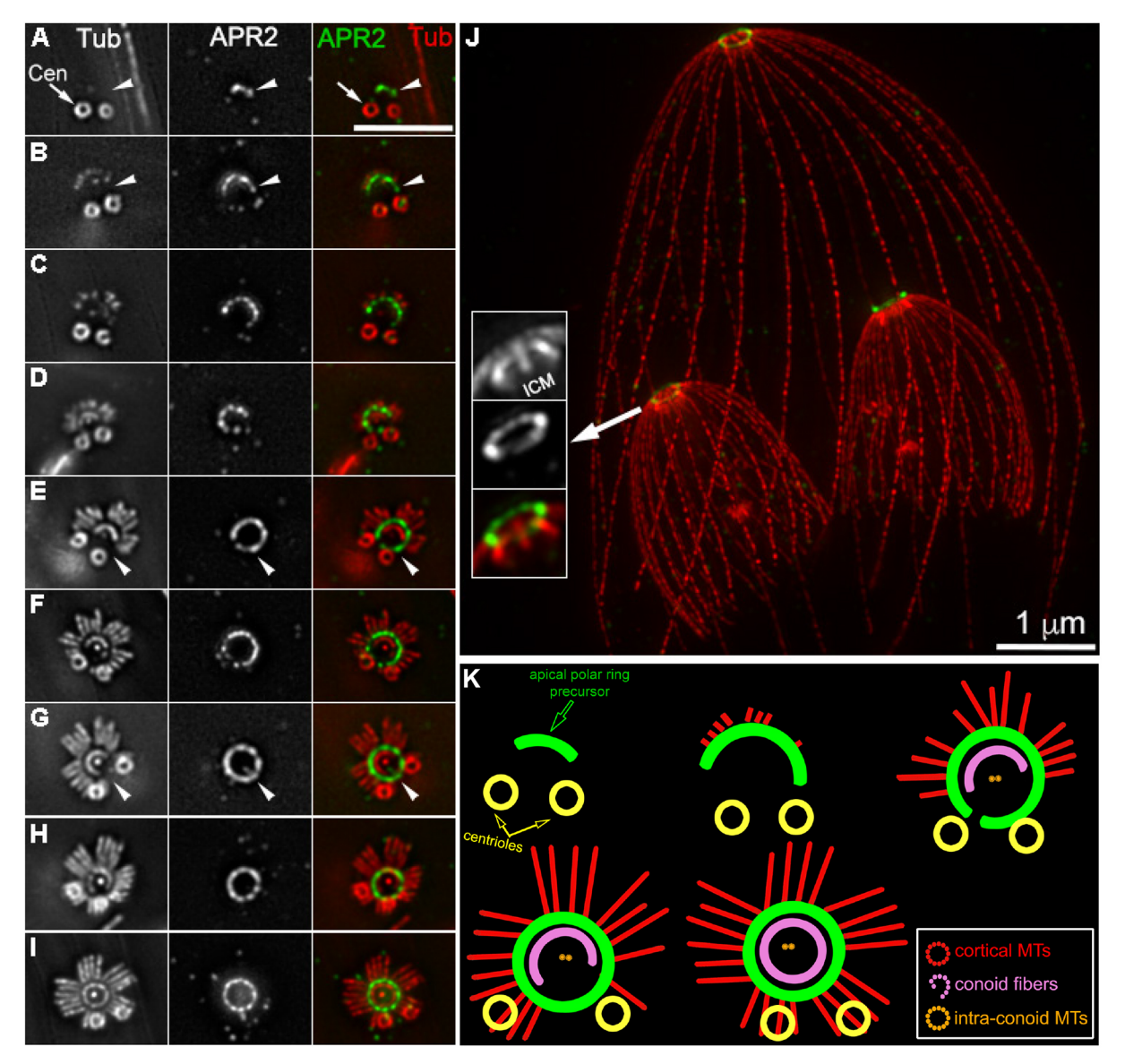


Fig. 3. The apical polar ring extends ahead of the cortical MT array during early daughter development. (A–J) Projections of ExM images of *mE-APR2* knock-in *Toxoplasma* parasites labeled with anti-tubulin (grayscale and red) and anti-GFP (grayscale and green, for APR2) antibodies. (A) Images of the centriole region before the daughter tubulin cytoskeleton appears. (B–I) Images of nascent daughter parasites ordered based on the number and length of cortical MTs. (J) Image of a dividing parasite with dome-shaped daughters. Insets in J (at twice the magnification of the main image) are projections of a subset of the sections showing that the apical polar ring labeling is positioned apically to the retracted daughter conoid. ICM, intra-conoid MTs. Image contrast was adjusted to optimize display. Arrowheads indicate sections of the apical polar ring that extend towards the centriole region beyond the forming MT array. Cen, centrioles. Scale bars: ≈1 μm before expansion. (K) Diagrams illustrating the development of cortical MTs (red), conoid (pink) and intra-conoid MTs (orange) with respect to that of the apical polar ring (green) in the vicinity of the centrioles (yellow). Diagrams were drawn based on images in A, B, E, G and I. Images in the figure were selected as most clearly representing the relevant features, chosen from 3D stacks of 124 parasites in two experiments.

mE-APR2 knock-in line by Cre-LoxP based excision, as described for $\Delta apr2$ (Fig. 2A).

We examined the number and arrangement of the MTs in the array in the wild-type parental line (RH $\Delta hx\Delta hu80$ – denoted 'RH $\Delta hu80$ ' or WT in what follows), $\Delta kinesinA$, $\Delta apr2$ and $\Delta kinesinA\Delta apr2$ parasites using ExM and anti-tubulin immunofluorescence (Fig. 7A,B). MT detachment or severe MT disorganization was detected in 0% of the mature WT parasites (total 727 parasites counted in three independent experiments), 2% of the $\Delta kinesinA$ (722 counted), 0.4% of the $\Delta apr2$ (545 counted) and 10% of the $\Delta kinesinA\Delta apr2$ (567 counted) parasites. The impact of the double knockout of KinesinA and APR2 is therefore more pronounced than the additive effect of the single knockouts,

but it is still very mild. Much more severe MT detachment occurs in the $\Delta kinesinA\Delta apr1$ parasite (86.6%, 156 counted), indicating that APR1 plays a more prominent role in reinforcement of the apical polar ring than APR2 (Fig. 7A).

To determine how the loss of KinesinA and APR2 affects the structure of the apical polar ring, we examined the wild-type parental, $\Delta kinesinA$, $\Delta apr2$ and $\Delta kinesinA\Delta apr2$ parasites by electron microscopy (EM) using negative staining after Triton X-100 (TX-100) extraction (Fig. 7C). We found that the removal of APR2 alone does not have a detectable impact. In the $\Delta kinesinA\Delta apr2$ parasites, the annulus associated with the roots of the cortical MTs traditionally recognized as the apical polar ring (Fig. 7C, arrowheads) is not detectable. This is likely solely due to the loss of KinesinA, because,

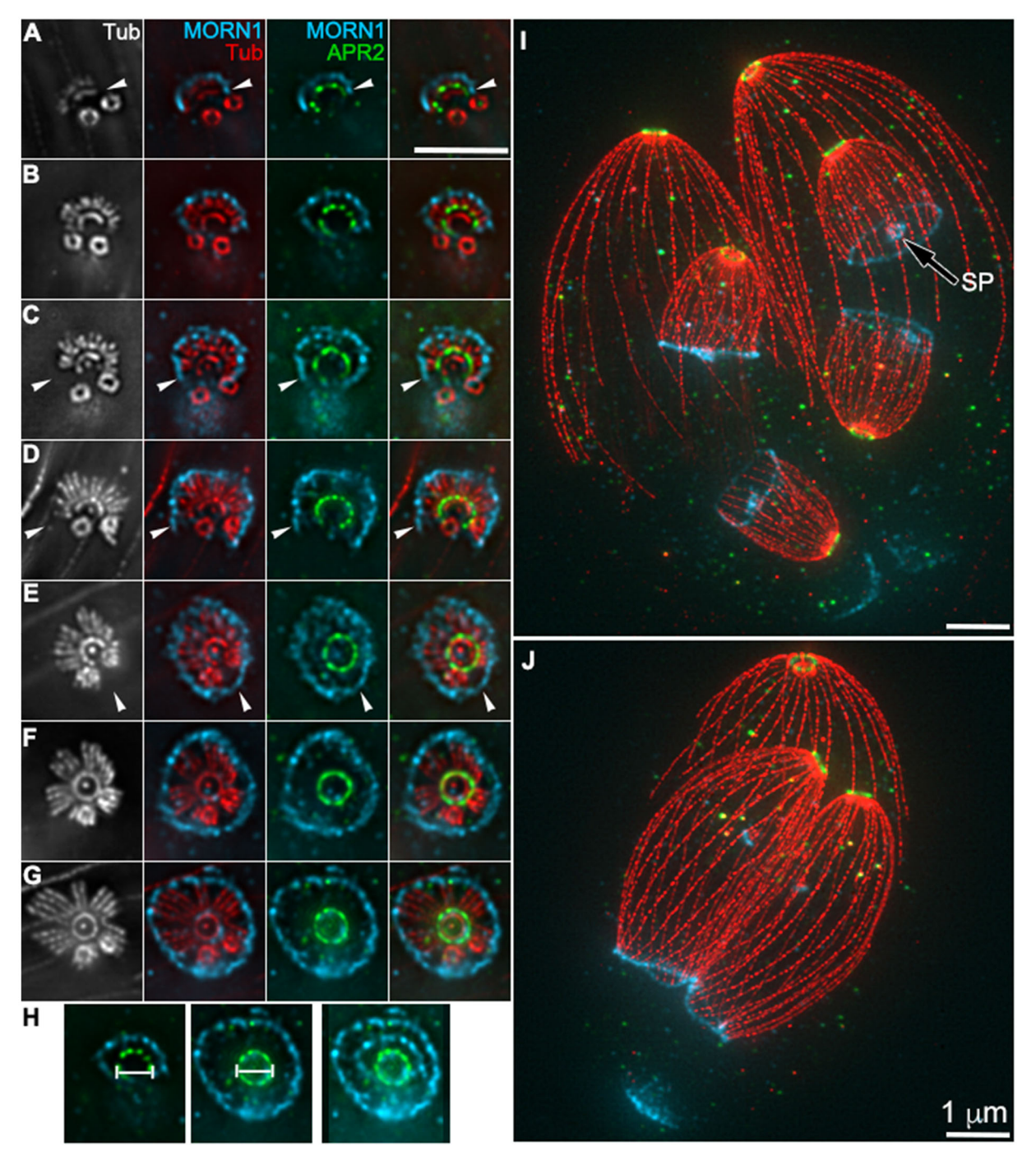


Fig. 4. The basal complex co-develops with the cortical MT array and the apical polar ring. (A–G,I,J) Projections of ExM images of mE-APR2 knock-in Toxoplasma parasites labeled using anti-tubulin (grayscale and red), anti-GFP (green, for APR2) and anti-MORN1 (cyan) antibodies. (A–G) Images of nascent daughter parasites ordered based on the number and length of cortical MTs. (I,J) Images of dividing parasites with dome-shaped daughters. Arrowheads indicate sections of the basal complex that extend towards the centriole region beyond the forming MT array. Black arrow in I indicates the spindle pole (SP). (H) A comparison of the daughter apical polar ring and basal complex labelings in B and G. The near-constant radius of the APR2 arc and/or ring is demonstrated using the reference bar. The increase of the radius of the MORN1 arc and/or ring is evident in the super-imposed image on the right. Image contrast was adjusted to optimize display. Scale bars: ≈1 µm before expansion. Scale bar in A applies to A–H. Images in the figure were selected as most clearly representing the relevant features, chosen from 3D stacks of 123 parasites in two experiments.

as previously reported, the removal of KinesinA alone also results in the loss of this band.

Using plaque assays, we assessed the ability of $\Delta kinesinA$, $\Delta apr2$ and $\Delta kinesinA\Delta apr2$ parasites to infect and destroy host cells relative to their parental line (Fig. 7D,E). We found that the plaquing

efficiency of $\Delta kinesinA$ and $\Delta apr2$ is ~70% and 108% of the parental RH $\Delta ku80$ (WT) line, respectively. In contrast, the plaquing efficiency of $\Delta kinesinA\Delta apr2$ is ~6.6%, far lower than the ~74% expected if the effects of the deletion of the two genes were simply additive.

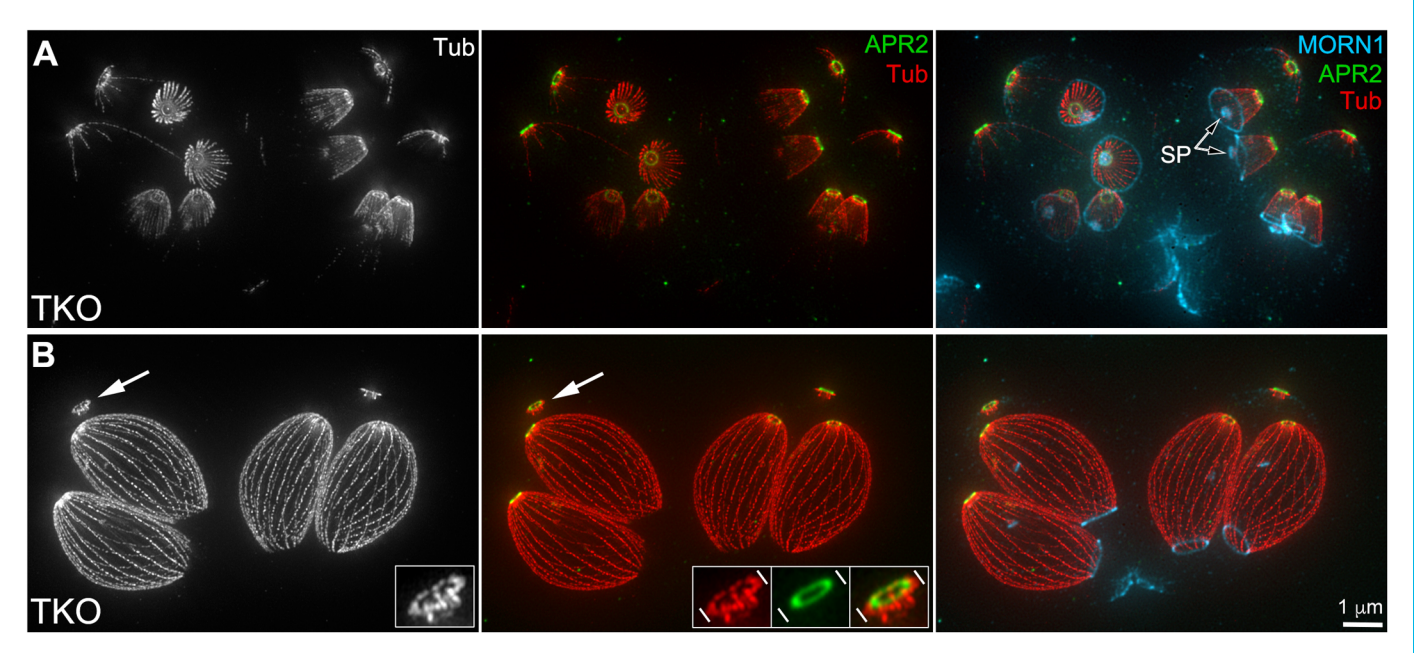


Fig. 5. The basal complex, cortical MT array and the apical polar ring assemble normally in the $\Delta t lap 2 \Delta spm1 \Delta t lap3$ parasites. (A,B) Projections of ExM images of $\Delta t lap 2 \Delta spm1 \Delta t lap3$ (TKO) parasites expressing mE-APR2 labeled with anti-tubulin (grayscale and red), anti-GFP (green, for APR2) and anti-MORN1 (cyan) antibodies. Black arrows indicate the spindle pole (SP). The panels include vacuoles containing parasites at earlier (A) and late (B) stages. Insets are at three times the magnification of the main image and include the parasite apex indicated by the white arrows. A remnant tubulin 'collar' around the apical polar ring is seen. White lines indicate the boundary of the tubulin collar. Image contrast was adjusted to optimize display. Scale bar: $\approx 1 \mu m$ before expansion (applies to both A and B). Images in the figure were selected as most clearly representing the relevant features, chosen from 3D stacks of 96 parasites in two experiments.

Invasion and egress are two essential steps in the lytic cycle. We compared the invasion efficiency of the $\Delta kinesinA\Delta apr2$ parasite with the wild-type parental and the single knockout parasites by using a dual-color assay that distinguishes the intraand extracellular parasite based on accessibility of the surface antigen P30 (Carey et al., 2004; Mital et al., 2005). We found that the invasion efficiency of $\Delta kinesinA\Delta apr2$ parasites is ~34% of that of wild-type parasites, again indicating a synergistic effect of the knockout of KinesinA and APR2, because it is lower than the predicted invasion efficiency (0.78×0.66=51%) of the $\Delta kinesin A \Delta apr 2$ parasites if the effect were simply additive (Table 1). We also assessed egress efficiency of the $\Delta kinesinA\Delta apr2$ parasite by an induced-egress assay, in which the infected cultures were treated with 5 μ M A23187, a Ca²⁺ ionophore. We found that there is no significant difference in the speed of parasite dispersal between the $\Delta kinesinA\Delta apr2$ and the parental parasites (Fig. 7F). A key process when the parasite switches between the intra- and extracellular states is secretion from the membrane-bound organelles (micronemes). To determine the impact of loss of KinesinA and APR2 on microneme secretion, we examined the secretion of the major adhesin, MIC2 (Microneme Protein 2) (Carruthers et al., 2000), and found that the A23187-induced MIC2 secretion of the $\Delta kinesinA\Delta apr2$ parasite remains robust (Fig. 7G; Fig. S2).

DISCUSSION

Several components of the apical polar ring have been identified previously (Tran et al., 2010; Katris et al., 2014; Leung et al., 2017; Barylyuk et al., 2020; Koreny et al., 2021), but only KinesinA was shown to be recruited to early daughters (Leung et al., 2017). Here, we show that APR2 is another early component of the apical polar ring. The knockout of APR2 alone has no impact on the parasite lytic cycle or MT arrangement. However, it appears to act synergistically with KinesinA. The knockout of KinesinA or

APR2 individually has a modest or no impact, but the removal of both components results in a severely impeded lytic cycle. In a significant minority of the $\Delta kinesinA\Delta apr2$ parasites, the cortical MTs are detached from the apex. A synergistic effect was also observed when Kinesin A and APR 1 were both knocked out, although the MT detachment phenotype here is significantly more severe. It is worth noting that APR1 becomes detectable only in the apical polar ring of relatively late daughters (Leung et al., 2017; Padilla et al., 2024). The knockout phenotype shows that APR1 is important for the stability of the MT-apical polar ring connection, so this late recruitment of APR1 indicates a need for additional stabilization of the MT array against the stress exerted by cortex expansion and growth as the daughter develops. Previous structural studies showed that the apical polar ring contains several substructures (Koreny et al., 2021; Gui et al., 2023). Comparison of the localization of RNG1 and APR2 revealed that these proteins belong to two distinct substructures with drastically different sensitivity to perturbations. In the $\Delta kinesinA\Delta apr1$ parasite, the RNG1 labeling fragments, but the APR2 ring remains intact. The $\Delta kinesinA\Delta apr1$ parasite therefore provides a convenient genetic background for assigning various apical polar ring components to different structural domains.

As the anchoring structure for the minus ends of the cortical MTs, the apical polar ring provides a model for exploring two basic cellular processes: the formation of a ring-like cytoskeletal structure and the patterning of a defined MT array. A well-studied example of a cytoskeletal ring-like structure is the actin-myosin-based contractile ring in yeast and mammalian cells (Hales et al., 1999; Mangione and Gould, 2019). This type of structure is 'born' as a ring through the preferential polymerization of the cytoskeletal filaments at the division plane. Here, using APR2 as the marker, we show that the assembly of the apical polar ring proceeds incrementally. The ring precursor first appears as a short arc, which extends towards the centriole region and eventually forms a closed

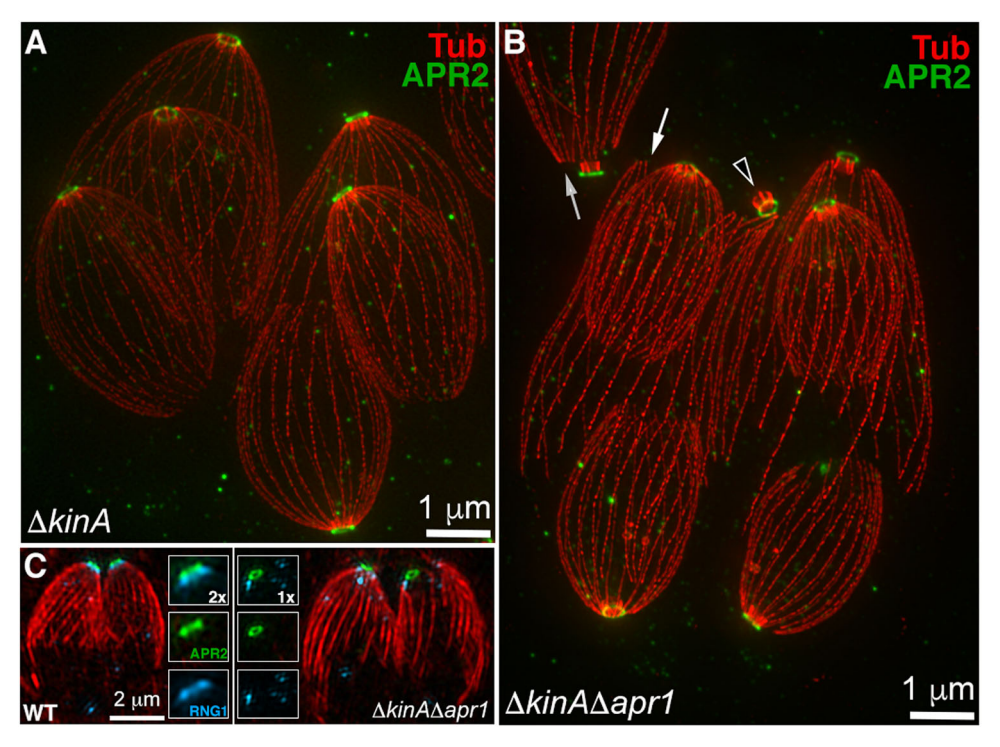


Fig. 6. The apical polar ring contains distinct substructures with different sensitivity to perturbations. (A) Projections of ExM images of $\Delta kinesinA$: mE-APR2 knock-in parasites labeled with anti-tubulin (red) and anti-GFP (green, for APR2) antibodies. Images in the figure were selected as most clearly representing the relevant features, chosen from 3D stacks of 50 parasites in one experiment. Scale bar: $\approx 1 \, \mu m$ prior to expansion. (B) Projections of ExM images of $\Delta kinesinA\Delta apr1$: mE-APR2 knock-in parasites labeled with anti-tubulin (red) and anti-GFP (green, for APR2) antibodies. White arrows indicate detached MTs. Arrowhead indicates a detached conoid. Images in the figure were selected as most clearly representing the relevant features, chosen from 3D stacks of 61 parasites in one experiment. Scale bar: $\approx 1 \, \mu m$ prior to expansion. (C) Projections of SIM images of mE-APR2 knock-in (WT) and $\Delta kinesinA\Delta apr1$: mE-APR2 knock-in ($\Delta kinesinA\Delta apr1$) parasites expressing RNG1-mCherry. Red indicates anti-tubulin staining; green indicates mE-APR2; cyan indicates RNG1-mCherry. Insets are shown at the indicated magnification. Images in the figure were selected as most clearly representing the relevant features, chosen from 3D stacks of 72 mE-APR2 knock-in parasites and 90 $\Delta kinesinA\Delta apr1:mE-APR2$ knock-in parasites in two experiments. Scale bar: 2 μm . Image contrast was adjusted to optimize display.

ring. The arc of the future apical polar ring progresses ahead of the step-wise nucleation of the MT array. This pattern is consistent with the apical polar ring laying down initiation sites for subsequent MT polymerization. It was recently reported that, in addition to localizing to the centrioles as previously described (Suvorova et al., 2015), γ-tubulin is also located at the spindle pole, the conoid, and the apical polar ring region (Engelberg et al., 2024 preprint; Haase et al., 2024). The knockdown of γ -tubulin annihilates the formation of almost all tubulin-containing structures, including the cortical MTs, the conoid and the spindle (Engelberg et al., 2024 preprint; Haase et al., 2024). This indicates that y-tubulin is involved in general MT nucleation, but it cannot in itself specify the distinct location and patterning that distinguishes different tubulin-containing structures. We propose that the specificity of the origination of the cortical MT array is coded in the apical polar ring through certain scaffold proteins that recruit nucleating factors such as γ-tubulin. So far, scaffold components that grossly affect the initial cortical MT patterning have not been identified. This calls for a much more thorough compilation of the composition and function of the apical polar ring.

The apical polar ring+cortical MT arrangement is ubiquitous among the apicomplexans. On the other hand, the cortical MT array displays species- and life stage-specific variations that coincide with major differences in life-cycle stages and physiology. For example, the mature *Plasmodium* ookinete has an intricate cage of ~60 cortical MTs, but the asexual blood-stage parasites only have a band of two to four cortical MTs (Garnham et al., 1962; Bannister et al., 2000; Morrissette and Sibley, 2002; Bounkeua et al., 2010; Wang et al.,

2020). Identifying the patterning factors in the apical polar ring of *Toxoplasma* will fuel related research in other apicomplexans, which in turn will provide further insights into how specific architectures of the MT array are achieved. For example, it would be intriguing to know whether the variations in the apicomplexan MT arrays are encoded in 'ruler' proteins in the apical polar ring that determine the spacing between the nucleation sites.

Remarkably, the assembly of the basal complex, which is located at the opposite end of the parasite from the apical polar ring, follows essentially the same pattern both in terms of timing and direction. This indicates that the assembly of not only the MT array, but also the apical-basal axis is dictated by a shared responsiveness to the same signal or shared recognition of some structural gradient. Given that the assembly invariably proceeds towards the centrioles, it is conceivable that the shared element is coded in the centrioles and/ or associated structures. A known structural connection between the centrioles and the daughter cytoskeletal framework is the striated fiber assemblins (SFA) fiber that links the centrioles with the daughter apical complex (Francia et al., 2012). However, the impact of the fiber seems to be at the level of triggering the initiation rather than dictating the direction of the assembly, because the formation of daughter parasites is inhibited when the SFA proteins are knocked down (Francia et al., 2012).

Similar to the apical polar ring, the basal complex also grows ahead of the MT array. The basal arc fully develops into a ring before all MTs are nucleated. This suggests that the formation of the basal ring is not dependent on the development of the MT array even though

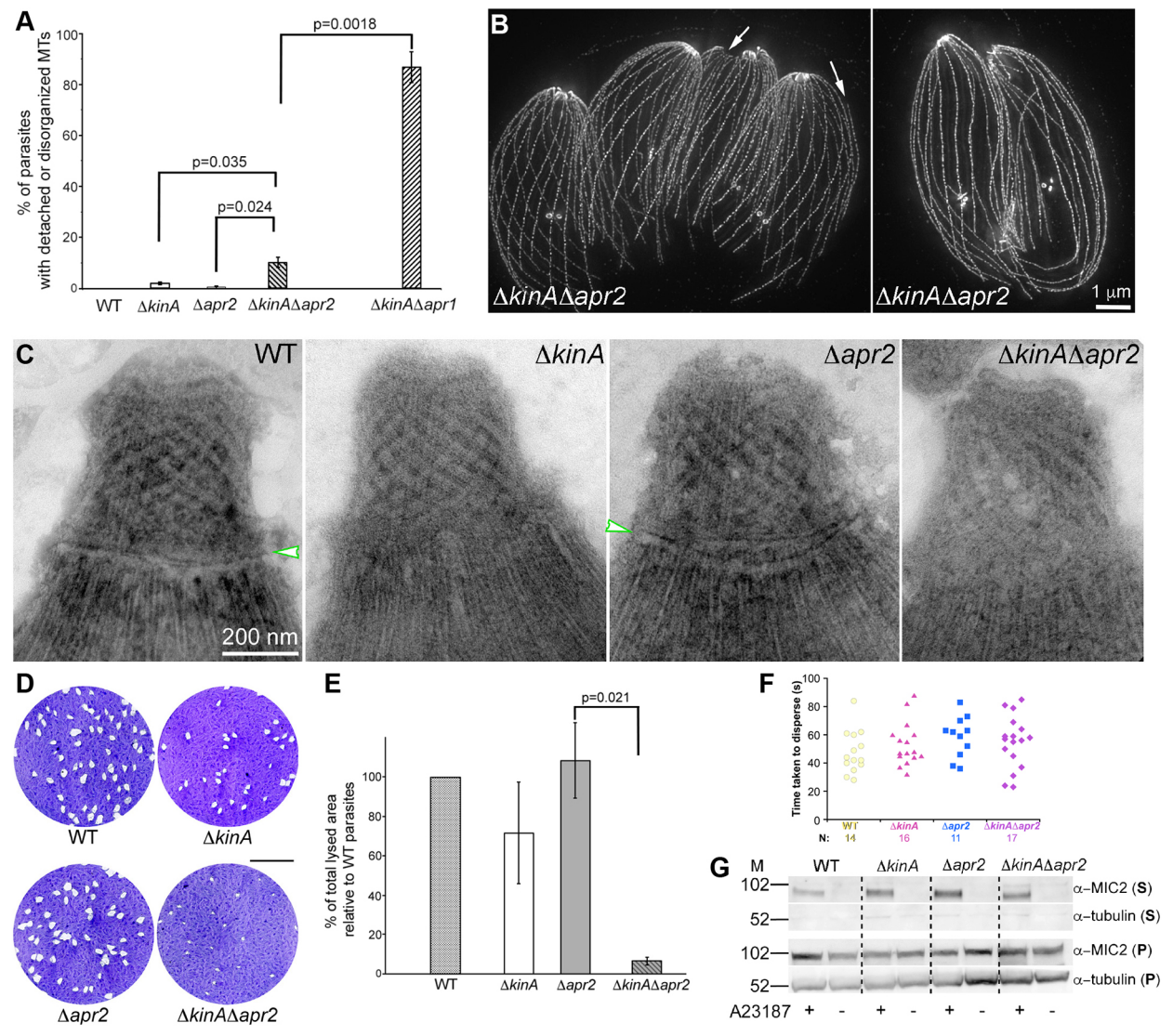


Fig. 7. The impact of APR2 and KinesinA on the organization of the cortical MTs, the apical polar ring and the parasite lytic cycle. (A) Bar graphs that compare the percentage of parasites with disorganized or detached cortical MTs in the RHAku80 parental (WT), AkinesinA (AkinA), Aapr2, ∆kinesinA∆apr2 and ∆kinesinA∆apr1 parasites. Data are presented as the mean±s.e.m. of three experiments (see main text for parasites per experiment). P-values were calculated using an unpaired two-tailed Student's t-test. (B) Projections of ExM images of \(\Delta \text{kinesinA} \text{apr2} \) parasites labeled using an antitubulin antibody as examples of normal and abnormal MT arrays. Left image indicates a vacuole that contains several parasites with detached MTs (arrows). Right image indicates two parasites with disorganized MTs. Scale bar: ≈1 µm before expansion. These images are shown as examples of ∆kinesinA∆apr2 parasites with MT defects, which are a minority of the population (see A), and are selected from three experimental repeats. (C) Negative-staining EM images of TX-100 extracted RH $\Delta ku80$ parental (WT), $\Delta kinesinA$, $\Delta apr2$ and $\Delta kinesinA\Delta apr2$ parasites. Arrowheads indicate the annulus associated with the roots of the cortical MTs traditionally recognized as the apical polar ring. This band is undetectable in \(\Delta kinesinA \) and \(\Delta kinesinA \Delta pr2 \) parasites. Images are representative of two experiments. (D) Plaque assays of the RHΔku80 parental (WT), ΔkinesinA, Δapr2 and ΔkinesinAΔapr2 parasites. Plaques are generated by cycles of parasite invasion, replication and egress that destroy the host cells. Scale bar: 1 cm. (E) Bar graphs that compare the percentage of the total lysed area (i.e. plaquing efficiency) relative to the wild-type parasites for WT (reference), ΔkinesinA, Δapr2 and ΔkinesinAΔapr2 parasites. Three independent experiments were conducted. Data are mean±s.e.m. P-values were calculated using an unpaired two-tailed Student's t-test. (F) Dot plots of time taken to disperse after treatment with 5 µM A23187 for the RHΔku80 parental (WT), ΔkinesinA, Δapr2 and ΔkinesinAΔapr2 parasites. The datasets for the Δ kinesinA and Δ kinesinA Δ apr2 parasites each contained one outlier with a dispersal time higher than 140 s, which are not included in the dot plots. (G) Western blots of the secreted (S) and pellet (P) fractions of RHΔku80 parental (WT), ΔkinesinA, Δapr2 and ΔkinesinAΔapr2 parasites with (+) or without (-) A23187 treatment, detected using anti-MIC2 and anti-tubulin antibodies. M indicates molecular mass markers (kDa). Image contrast was enhanced and inverted to aid visualization. See Fig. S2 for the full blots. Blots shown are representative of three experiments.

they are constructed in concert. Consistent with this interpretation, we found previously that the MORN1 ring still forms when daughter MT polymerization is inhibited by oryzalin treatment (Hu, 2008). Furthermore, when ectopically expressed in bacteria, MORN1 forms into rings by itself (Heaslip et al., 2010). However, despite its intrinsic ability to polymerize into a ring, MORN1 in *Toxoplasma* assembles only into the basal complex at the distal end of the forming daughters,

where the plus-end of the cortical MTs is located. Because the ring-forming activity of MORN1 is not dependent on MT polymerization or membrane association, the specific localization of MORN1 to the basal end of the daughter is almost certainly due to bridge proteins. One would also predict that the removal of these bridge proteins should result in a displaced MORN1 ring due to decoupling. So far, no such proteins have been identified.

Table 1. Quantification of invasion for four T. gondii lines

Strain	Mean number invaded±s.e.m	Percentage of wild type	RH∆ku80 (wild type)	∆kinesinA	∆apr2	∆kinesinA∆apr2
RH∆ku80 (wild type)	72.1±8.0	100	_	P=0.17	P=0.04	P=0.01
ΔkinesinA	56±8.5	78	_	_	P=0.38	P=0.03
∆apr2	47.3±6.4	66	_	_	_	P=0.04
∆kinesinA∆apr2	24.6±6.6	34	_	_	-	_

The number of intracellular parasites per field was counted in 20 fields per strain in each of three independent biological replicates. *P*-values were calculated using an unpaired two-tailed Student's *t*-test.

It has been proposed that the apical complex might have originated from structures associated with a flagellum (Portman and Slapeta, 2014). The molecular link includes a number of shared components, such as centrin, dynein light chain (DLC), SAS6-like protein and MORN-domain containing protein, as well as the SFA fiber that connects the centrioles with the daughter apical complex (Hu et al., 2006; Francia et al., 2012; de Leon et al., 2013). In other eukaryotes, SFA proteins form the striated rootlet that associates with the basal body. The potential evolutionary connection between the apical complex and the flagellum is further supported by the structural analysis of Chromera, which showed that the pseudoconoid, structural 'homolog' of the conoid is located close to the basal body of one of the two flagella (Portman et al., 2014; Portman and Slapeta, 2014). Interestingly, some of the proteins that suggest a molecular link between the apical complex and flagellum are also found in the basal complex, such as centrin 2, DLC and MORN1 (Hu et al., 2006). It is therefore worth considering that the basal complex is also a reduced and altered flagellum-related structure. If the apical and basal complexes were indeed derived from a di-flagella architecture, this could explain both their shared molecular composition and their highly coordinated construction.

MATERIALS AND METHODS

T. gondii cultures and transfection

T. gondii tachyzoites were cultured and transfected as described previously (Roos et al., 1994; Liu et al., 2015; Leung et al., 2017; Munera Lopez et al., 2022).

Plasmid construction

Genomic DNA (gDNA) and coding sequences (CDS) were prepared as described previously (Munera Lopez et al., 2022).

For the pTKO2_II-mEmerald-APR2 (mE-APR2) knock-in, ~1.9 kb fragments upstream (5'UTR) or downstream (3'UTR) of the APR2 (TGGT1_227000) genomic locus were amplified from the parasite genomic DNA by PCR using primers S1 and AS1 (5'UTR), and S2 and AS2 (for 3' UTR), and inserted at the NotI (5'UTR) or HindIII (3'UTR) site of plasmid pTKO2-II-mCherryFP (Liu et al., 2013) using the NEBuilder HiFi Assembly kit. The CDS for mEmeraldFP-APR2 was HiFi assembled into the AsiSI site of this construct, generating pTKO2_II-mE-APR2. The mEmeraldFP CDS was amplified using S3 and AS3. The CDS for APR2 was amplified using primers S4 and AS4, S5 and AS5, and S6 and AS6. A linker sequence encoding SGLRS was added between the APR2- and Emerald-coding sequences, and the Kozak sequence from the endogenous APR2 locus (TGGTGTCAGatg) was added to the 5' end of the mEmerald-coding sequence. The backbone of the pTKO2_II-mE-APR2 plasmid contains a cassette driving expression of cytoplasmic mCherryFP, to help identify and exclude non-homologous or single homologous recombinants (Liu et al., 2013). See Table S1 for primers used in PCR amplification

Generation of knock-in, endogenously tagged, knockout, complemented and transgenic parasites

To create the mE-APR2 knock-in line, $\sim 1 \times 10^7$ RH $\Delta hx\Delta ku80$ parasites were electroporated with 40 μ g of NotI linearized pTKO2_II-mE-APR2 and selected with 25 μ g/ml mycophenolic acid and 50 μ g/ml xanthine. Clones were screened for mE-APR2 fluorescence and for lack of cytoplasmic

mCherry fluorescence. Clones were confirmed by genomic PCRs and then by Southern blot. Clones verified by Southern blots were used in the generation of $\Delta apr2$ parasites.

For the $\Delta apr2$ line, mE-APR2 knock-in parasites were electroporated with 30 µg of pmin-Cre-eGFP_Gra-mCherry (Liu et al., 2015), selected with 80 µg/ml of 6-thioxanthine, and screened for the loss of mEmerald fluorescence. Clones were confirmed by genomic PCRs and then verified by Southern blot.

 $\Delta kinesinA: mE-APR2$ knock-in and $\Delta kinesinA\Delta apr1: mE-APR2$ knock-in lines were created by electroporating $\Delta kinesinA$ or the $\Delta kinesinA\Delta apr1$ parasites (Leung et al., 2017) with linearized pTKO2_II-mE-APR2 plasmid. The clones in which homologous recombination had occurred were selected and screened for, as described above for the mE-APR2 knock-in line.

 $\Delta kinesinA$: mE-APR2 knock-in parasites were electroporated with pmin-Cre-eGFP_Gra-mCherry to create the $\Delta kinesinA\Delta apr2$ line. Clones were selected and screened for as described above for the $\Delta apr2$ parasites.

RNG1-mCherry expressing $\Delta kinesinA\Delta apr1: mE-APR2$ knock-in parasites were created by electroporating $\Delta kinesinA\Delta apr1: mE-APR2$ knock-in parasites with pLIC-RNG1-mCherry linearized with EcoRV, then selecting with 1 μ M pyrimethamine for two passages until the population became drug resistant and cloning by limited dilution. pLIC-RNG1-mCherry was a kind gift from Dr. Naomi Morrissette (University of California, Irvine, USA) (Tran et al., 2010).

To create the mE-APR2 expressing TKO parasite, $\Delta tlap2\Delta tlap3\Delta spm1$ ('TKO') parasites (Liu et al., 2015) were electroporated with linearized pTKO2_II-mE-APR2 knock-in plasmid and selected with 25 µg/ml mycophenolic acid and 50 µg/ml xanthine. Clones were screened for mE-APR2 fluorescence and for lack of cytoplasmic mCherry fluorescence.

Southern blotting

The Southern blotting protocol was largely as described previously (Liu et al., 2013, 2015). To probe and detect changes in the APR2 genomic locus in the parental (RH $\Delta ku80\Delta hx$), mE-APR2 knock-in and $\Delta apr2$ parasites, 5 μ g of gDNA from each line was digested before hybridization with a 5'UTR, CDS or 3'UTR probe. Gel-purified templates for probe synthesis were generated by restriction digestions from the pTKO2_II-mE-APR2 knock-in plasmid: BstZ17I and PmeI digestion to release the template for the 5'UTR probe; AvrII and AfeI digestion to release the template for the CDS probe; HindIII and PspOMI digestion to release the template for the 3'UTR probe.

For hybridization with the 5'UTR probe, parasite genomic DNA was digested with MluI. The predicted MluI fragment sizes are 8687 bp for the parental, 6767 bp for the knock-in and 5146 bp for the knockout lines. For hybridization with the CDS probe, parasite genomic DNA was digested with BstBI. The predicted BstBI fragment sizes are 10994 bp and 4098 bp for the parental (i.e. wild-type apr2 locus) and 4327 bp for the knock-in. As expected, no signal was detected in the lane with $\Delta apr2$ genomic DNA when hybridized with the CDS probe. For hybridization with the 3'UTR probe, parasite genomic DNA was digested with AfeI. The predicted AfeI fragment sizes are 11754 bp for the parental, 6617 bp for the knock-in and 8404 bp for the knockout lines.

Three-dimensional structured illumination microscopy

Parasites were grown in HFF cells (kind gift from Dr David Roos, University of Pennsylvania, PA, USA) in glass-bottom dishes (MatTek, P35G-1.5-21-C). Before imaging, the cultures were placed in L15 imaging media [Leibovitz's L-15 (21083-027, Gibco- Life Technologies) supplemented

with 1% (vol/vol) heat-inactivated cosmic calf serum (CCS; SH30087.3, Hyclone)]. Samples were imaged with a DeltaVision OMX Flex imaging station (GE Healthcare-Applied Precision) as previously described (Padilla et al., 2024). Contrast levels were adjusted to optimize the display.

Sample preparation and imaging for ExM

ExM samples labeled with only anti-tubulin antibody were processed exactly as described by Padilla et al. (2024). In that protocol, Toxoplasma-infected monolayers of HFF cells on 12 mm round coverslips were pre-fixed with 3.6% formaldehyde (made from paraformaldehyde) in PBS for 15-30 min at room temperature before fixing in the anchoring solution (2% acrylamide and 1.4% formaldehyde in PBS) for ExM. Under this condition, the labeling of the apical polar ring in the mE-APR2 knock-in parasites using anti-GFP antibodies was weak. This is likely due to epitope masking, because omitting the pre-fixation step or adding TX-100 extraction during the pre-fixation step both significantly improve the anti-GFP signal. The preservation of parasite morphology and the strength of the anti-GFP signal were comparable between the two methods. For the latter method, Toxoplasma-infected monolayers of HFF cells on 12 mm round coverslips were fixed with 2.4% formaldehyde in PBS for 30 s followed by permeabilization with 0.4% TX-100 in PBS for 3 min. After washing twice with PBS for 5 min, the samples were fixed again with 2.4% formaldehyde in PBS for 20 min and washed twice for 5 min with PBS, followed by a second permeabilization with 0.2% TX-100 in PBS for 10 min and two additional washes for 5 min before incubation in the anchoring solution. This method is the same as that described by Louvel et al. (2023) for labeling nuclear pore complexes.

Tubulin labeling was carried out with a mouse monoclonal anti-acetylated tubulin antibody (T6793-6-11B-1, Sigma-Aldrich, 1:250) and followed by a goat anti-mouse IgG Cy3 (115-165-166, Jackson ImmunoResearch Labs, 1:400) or goat anti-mouse IgG 488 (A-11029, Invitrogen, 1:400). Labeling of mE-APR2 was carried out using rabbit anti-GFP antibody (Torrey Pine-TP401, 1:200), followed by goat anti-rabbit IgG Alexa488 (A-11034, Invitrogen, 1:400). Labeling of MORN1 was carried out using a rat anti-TgMORN1 antibody (Heaslip et al., 2010), followed by goat anti-rat IgG Cy5 (Jackson ImmunoResearch Labs 112-175-167). All other steps in ExM and antibody labeling were performed as previously described (Padilla et al., 2024).

Expanded samples were imaged as described previously (Padilla et al., 2024). Sum or maximum projections were presented in the figures. Contrast levels were adjusted to optimize the display. Estimation of the expansion ratio has been described previously (Padilla et al., 2024).

Electron microscopy

Suspensions of extracellular parasites were treated with A23187 and processed for negative staining as described previously (Munera Lopez et al., 2022). The negatively stained samples were imaged on a Talos transmission electron microscope (Thermo Fisher Scientific) at 120 keV.

Plaque assay

Freshly harvested parasites (100 per well) were used to infect confluent HFF monolayers in six-well plates. After incubation at 37°C for 7 days, the cultures were rinsed, fixed, stained and scanned as described previously (Munera Lopez et al., 2022). Three independent experiments were performed.

Invasion, egress and microneme secretion assays

Immunofluorescence-based invasion assays were carried out as described previously (Munera Lopez et al., 2022) with some modifications. Approximately 1×10^6 freshly egressed parasites were used to inoculate a MatTek dish of nearly confluent HFF cells. After 10 min incubation on ice and then 60 min incubation at 37° C, the samples were processed for immunofluorescence as described previously (Munera Lopez et al., 2022). Three biological replicates were performed. Parasites in 20 fields were counted for each strain per biological replicate. In total (intracellular+extracellular), 6230 parasites were counted for the RH Δhx parent, 4303 for $\Delta kinesinA$, 4616 for $\Delta apr2$ and 2877 for $\Delta kinesinA\Delta apr2$ parasites. P-values were calculated using an unpaired Student's t-test.

The induced egress assays were carried out as described previously (Munera Lopez et al., 2022). Microneme secretion assays and western blot

analysis were carried out as described in Tengganu et al. (2023) with a mouse 6D10 anti-TgMIC2 antibody (Carruthers et al., 2000) and a mouse anti-tubulin (Sigma, T6074) at 1:1000 and 1:4000 dilution, respectively.

Acknowledgements

We thank Matea Susac for tissue culture support and Isadonna F. Tengganu for helpful discussions, and Dr Dewight Williams at the Eyring Materials Center at ASU for EM support.

Competing interests

The authors declare no competing or financial interests.

Author contributions

Conceptualization: K.H., L.F.A.P., J.M.L., J.M.M.; Methodology: K.H., L.F.A.P., J.M.L., J.M.M.; Investigation: K.H., L.F.A.P., J.M.L., A.S.; Data curation: K.H., L.F.A.P., J.M.L., A.S.; Writing – original draft: K.H., L.F.A.P., J.M.L., J.M.M.; Writing – review & editing: L.F.A.P., J.M.L., J.M.M.; Supervision: K.H., J.M.M.; Project administration: K.H.; Funding acquisition: K.H.

Funding

This study was supported by funding from the National Institutes of Health National Institute of Allergy and Infectious Diseases (R01-Al132463 to K.H.) and from the National Science Foundation (2119963 to K.H. as co-PI). Deposited in PMC for release after 12 months.

Data availability

All relevant data can be found within the article and its supplementary information.

First Person

This article has an associated First Person interview with the co-first authors of the paper.

Peer review history

The peer review history is available online at https://journals.biologists.com/jcs/lookup/doi/10.1242/jcs.263436.reviewer-comments.pdf

References

- Bannister, L. H., Hopkins, J. M., Fowler, R. E., Krishna, S. and Mitchell, G. H. (2000). A brief illustrated guide to the ultrastructure of *Plasmodium falciparum* asexual blood stages. *Parasitol. Today* 16, 427-433. doi:10.1016/S0169-4758(00)01755-5
- Barylyuk, K., Koreny, L., Ke, H., Butterworth, S., Crook, O. M., Lassadi, I., Gupta, V., Tromer, E., Mourier, T., Stevens, T. J. et al. (2020). A Comprehensive Subcellular Atlas of the *Toxoplasma* Proteome via hyperLOPIT Provides Spatial Context for Protein Functions. *Cell Host Microbe* 28, 752-766.e9. doi:10.1016/j.chom.2020.09.011
- Bounkeua, V., Li, F. and Vinetz, J. M. (2010). In vitro generation of *Plasmodium falciparum* ookinetes. *Am. J. Trop. Med. Hyg.* 83, 1187-1194. doi:10.4269/ajtmh. 2010.10-0433
- Carey, K. L., Westwood, N. J., Mitchison, T. J. and Ward, G. E. (2004). A small-molecule approach to studying invasive mechanisms of *Toxoplasma gondii*. Proc. Natl. Acad. Sci. USA 101, 7433-7438. doi:10.1073/pnas.0307769101
- Carruthers, V. B., Sherman, G. D. and Sibley, L. D. (2000). The *Toxoplasma* adhesive protein MIC2 is proteolytically processed at multiple sites by two parasite-derived proteases. *J. Biol. Chem.* **275**, 14346-14353. doi:10.1074/jbc. 275.19.14346
- Checkley, W., White, A. C., Jr., Jaganath, D., Arrowood, M. J., Chalmers, R. M., Chen, X.-M., Fayer, R., Griffiths, J. K., Guerrant, R. L., Hedstrom, L. et al. (2015). A review of the global burden, novel diagnostics, therapeutics, and vaccine targets for *cryptosporidium*. *Lancet Infect. Dis.* 15, 85-94. doi:10.1016/S1473-3099(14)70772-8
- De Leon, J. C., Scheumann, N., Beatty, W., Beck, J. R., Tran, J. Q., Yau, C., Bradley, P. J., Gull, K., Wickstead, B. and Morrissette, N. S. (2013). A SAS-6-like protein suggests that the *Toxoplasma* conoid complex evolved from flagellar components. *Eukaryot. Cell* 12, 1009-1019. doi:10.1128/EC.00096-13
- Dubremetz, J. F. and Elsner, Y. Y. (1979). Ultrastructural study of schizogony of Eimeria bovis in cell cultures. J. Protozool. 26, 367-376. doi:10.1111/j.1550-7408. 1979 tb04639 x
- Engelberg, K., Bechtel, T., Michaud, C., Weerapana, E. and Gubbels, M. J. (2022). Proteomic characterization of the *Toxoplasma gondii* cytokinesis machinery portrays an expanded hierarchy of its assembly and function. *Nat. Commun.* 13, 4644. doi:10.1038/s41467-022-32151-0
- Engelberg, K., Bauwens, C., Ferguson, D. J. P. and Gubbels, M.-J. (2024). Co-dependent formation of the *Toxoplasma gondii* sub-pellicular microtubules and inner membrane skeleton. *bioRxiv*, 2024.2005.2025.595886. doi:10.1101/2024.05.25.595886

- Francia, M. E., Jordan, C. N., Patel, J. D., Sheiner, L., Demerly, J. L., Fellows, J. D., De Leon, J. C., Morrissette, N. S., Dubremetz, J.-F. and Striepen, B. (2012). Cell division in Apicomplexan parasites is organized by a homolog of the striated rootlet fiber of algal flagella. *PLoS Biol.* 10, e1001444. doi:10.1371/journal.pbio.1001444
- Frenkel, J. K. (1973). Toxoplasmosis: Parasite Life Cycle, Pathology, and Immunology. Baltimore, MD: University Park Press.
- Garnham, P. C., Bird, R. G. and Baker, J. R. (1962). Electron microscope studies of motile stages of malaria parasites. III. The ookinetes of *Haemamoeba* and *Plasmodium. Trans. R. Soc. Trop. Med. Hyg.* 56, 116-120. doi:10.1016/0035-9203(62)90137-2
- Gubbels, M., Vaishnava, S., Boot, N., Dubremetz, J. F. and Striepen, B. (2006). A MORN-repeat protein is a dynamic component of the *Toxoplasma gondii* cell division apparatus. *J. Cell Sci.* 119, 2236-2245. doi:10.1242/jcs.02949
- Gui, L., O'shaughnessy, W. J., Cai, K., Reetz, E., Reese, M. L. and Nicastro, D. (2023). Cryo-tomography reveals rigid-body motion and organization of apicomplexan invasion machinery. *Nat. Commun.* 14, 1775. doi:10.1038/s41467-023-37327-w
- Haase, R., Puthenpurackal, A., Maco, B., Guérin, A. and Soldati-Favre, D. (2024). γ-tubulin complex controls the nucleation of tubulin-based structures in Apicomplexa. *Mol. Biol. Cell* 35, ar121. doi:10.1091/mbc.E24-03-0100
- Hales, K. G., Bi, E., Wu, J. Q., Adam, J. C., Yu, I. C. and Pringle, J. R. (1999). Cytokinesis: an emerging unified theory for eukaryotes? *Curr. Opin. Cell Biol.* 11, 717-725. doi:10.1016/S0955-0674(99)00042-3
- Heaslip, A. T., Dzierszinski, F., Stein, B. and Hu, K. (2010). TgMORN1 is a key organizer for the basal complex of *Toxoplasma gondii*. *PLoS Pathog*. 6, e1000754. doi:10.1371/journal.ppat.1000754
- Hepler, P., Huff, C. and Sprinz, H. (1966). The fine structure of the exoerythrocytic stages of *Plasmodium fallax*. J. Cell Biol. 30, 333-359. doi:10.1083/icb.30.2.333
- Hu, K. (2008). Organizational changes of the daughter basal complex during the parasite replication of *Toxoplasma gondii*. PLoS Pathog. 4, e10. doi:10.1371/journal.ppat.0040010
- Hu, K., Mann, T., Striepen, B., Beckers, C. J., Roos, D. S. and Murray, J. M. (2002a). Daughter cell assembly in the protozoan parasite *Toxoplasma gondii*. *Mol. Biol. Cell* 13, 593-606. doi:10.1091/mbc.01-06-0309
- Hu, K., Roos, D. S. and Murray, J. M. (2002b). A novel polymer of tubulin forms the conoid of *Toxoplasma gondii*. J. Cell Biol. 156, 1039-1050. doi:10.1083/jcb. 200112086
- Hu, K., Johnson, J., Florens, L., Fraunholz, M., Suravajjala, S., Dilullo, C., Yates, J., Roos, D. S. and Murray, J. M. (2006). Cytoskeletal components of an invasion machine the apical complex of *Toxoplasma gondii*. *PLoS Pathog.* 2, e13. doi:10. 1371/journal.ppat.0020013
- Katris, N. J., Van Dooren, G. G., Mcmillan, P. J., Hanssen, E., Tilley, L. and Waller, R. F. (2014). The apical complex provides a regulated gateway for secretion of invasion factors in *Toxoplasma*. *PLoS Pathog*. **10**, e1004074. doi:10. 1371/journal.ppat.1004074
- Koreny, L., Zeeshan, M., Barylyuk, K., Tromer, E. C., Van Hooff, J. J. E., Brady, D., Ke, H., Chelaghma, S., Ferguson, D. J. P., Eme, L. et al. (2021). Molecular characterization of the conoid complex in *Toxoplasma* reveals its conservation in all apicomplexans, including *Plasmodium* species. *PLoS Biol.* 19, e3001081. doi:10.1371/journal.pbio.3001081
- Leung, J. M., He, Y., Zhang, F., Hwang, Y. C., Nagayasu, E., Liu, J., Murray, J. M. and Hu, K. (2017). Stability and function of a putative microtubule organizing center in the human parasite *Toxoplasma gondii*. Mol. Biol. Cell 28, 1361-1378. doi:10.1091/mbc.E17-01-0045
- Li, Z., Du, W., Yang, J., Lai, D.-H., Lun, Z.-R. and Guo, Q. (2023). Cryo-electron tomography of toxoplasma gondii indicates that the conoid fiber may be derived from microtubules. Adv Sci 10, 2206595. doi:10.1002/advs.202206595
- Liu, J., Wetzel, L., Zhang, Y., Nagayasu, E., Ems-Mcclung, S., Florens, L. and Hu, K. (2013). Novel thioredoxin-like proteins are components of a protein complex coating the cortical microtubules of *Toxoplasma gondii*. Eukaryot. Cell 12, 1588-1599. doi:10.1128/EC.00082-13
- Liu, J., He, Y., Benmerzouga, I., Sullivan, W. J., Jr., Morrissette, N. S., Murray, J. M. and Hu, K. (2015). An ensemble of specifically targeted proteins stabilizes cortical microtubules in the human parasite *Toxoplasma gondii*. Mol. Biol. Cell 27, 549-571. doi:10.1091/mbc.E15-11-0754
- Lorestani, A., Sheiner, L., Yang, K., Robertson, S. D., Sahoo, N., Brooks, C. F., Ferguson, D. J., Striepen, B. and Gubbels, M. J. (2010). A *Toxoplasma* MORN1 null mutant undergoes repeated divisions but is defective in basal assembly, apicoplast division and cytokinesis. *PLoS One* 5, e12302. doi:10.1371/journal.pone.0012302
- Louvel, V., Haase, R., Mercey, O., Laporte, M. H., Eloy, T., Baudrier, É., Fortun, D., Soldati-Favre, D., Hamel, V. and Guichard, P. (2023). iU-ExM: nanoscopy of

- organelles and tissues with iterative ultrastructure expansion microscopy. *Nature Commun.* **14**, 7893. doi:10.1038/s41467-023-43582-8
- Lyons, R. E., Mcleod, R. and Roberts, C. W. (2002). Toxoplasma gondii tachyzoite-bradyzoite interconversion. Trends Parasitol. 18, 198-201. doi:10. 1016/S1471-4922(02)02248-1
- Mangione, M. C. and Gould, K. L. (2019). Molecular form and function of the cytokinetic ring. *J. Cell Sci.* 132, jcs226928. doi:10.1242/jcs.226928
- Mital, J., Meissner, M., Soldati, D. and Ward, G. E. (2005). Conditional expression of *Toxoplasma gondii* apical membrane antigen-1 (TgAMA1) demonstrates that TgAMA1 plays a critical role in host cell invasion. *Mol. Biol. Cell* 16, 4341-4349. doi:10.1091/mbc.e05-04-0281
- Morrissette, N. S. and Sibley, L. D. (2002). Cytoskeleton of apicomplexan parasites. Microbiol. Mol. Biol. Rev. 66, 21-38. doi:10.1128/MMBR.66.1.21-38.2002
- Morrissette, N. S., Murray, J. M. and Roos, D. S. (1997). Subpellicular microtubules associate with an intramembranous particle lattice in the protozoan parasite *Toxoplasma gondii. J. Cell Sci.* **110**, 35-42. doi:10.1242/jcs.110.1.35
- Munera Lopez, J., Tengganu, I. F., Liu, J., Murray, J. M., Arias Padilla, L. F., Zhang, Y., Brown, P. T., Florens, L. and Hu, K. (2022). An apical protein, Pcr2, is required for persistent movement by the human parasite *Toxoplasma gondii*. PLoS Pathog. 18, e1010776. doi:10.1371/journal.ppat.1010776
- Nichols, B. A. and Chiappino, M. L. (1987). Cytoskeleton of *Toxoplasma gondii*. *J. Protozool.* **34**, 217-226. doi:10.1111/j.1550-7408.1987.tb03162.x
- Padilla, L. F. A., Murray, J. M. and Hu, K. (2024). The initiation and early development of the tubulin-containing cytoskeleton in the human parasite Toxoplasma gondii. Mol. Biol. Cell 35, ar37. doi:10.1091/mbc.E23-11-0418
- Portman, N. and Slapeta, J. (2014). The flagellar contribution to the apical complex: a new tool for the eukaryotic Swiss Army knife? *Trends Parasitol.* 30, 58-64. doi:10.1016/j.pt.2013.12.006
- Portman, N., Foster, C., Walker, G. and Slapeta, J. (2014). Evidence of intraflagellar transport and apical complex formation in a free-living relative of the apicomplexa. *Eukaryot. Cell* 13, 10-20. doi:10.1128/EC.00155-13
- Roos, D. S., Donald, R. G., Morrissette, N. S. and Moulton, A. L. (1994).
 Molecular tools for genetic dissection of the protozoan parasite *Toxoplasma gondii*. Methods Cell Biol. 45, 27-78. doi:10.1016/S0091-679X(08)61845-2
- Russell, D. G. and Burns, R. G. (1984). The polar ring of coccidian sporozoites: a unique microtubule-organizing centre. J. Cell Sci. 65, 193-207. doi:10.1242/jcs. 65.1.193
- Seeber, F. and Steinfelder, S. (2016). Recent advances in understanding apicomplexan parasites. F1000Res. 5, F1000 Faculty Rev-1369. doi:10.12688/ f1000research.7924.1
- Sheffield, H. G. (1970). Schizogony in *Toxoplasma gondii*: an electron microscope study. *Proc. Helminth. Soc. Wash.* 37, 237-242.
- Sheffield, H. G. and Melton, M. L. (1968). The fine structure and reproduction of Toxoplasma gondii. J. Parasitol. 54, 209-226. doi:10.2307/3276925
- Sun, S. Y., Segev-Zarko, L.-A., Chen, M., Pintilie, G. D., Schmid, M. F., Ludtke, S. J., Boothroyd, J. C. and Chiu, W. (2022). Cryo-ET of *Toxoplasma* parasites gives subnanometer insight into tubulin-based structures. *Proc. Natl. Acad. Sci. USA* 119, e2111661119. doi:10.1073/pnas.2111661119
- Suvorova, E. S., Francia, M., Striepen, B. and White, M. W. (2015). A novel bipartite centrosome coordinates the apicomplexan cell cycle. *PLoS Biol.* 13, e1002093. doi:10.1371/journal.pbio.1002093
- Tengganu, I. F., Arias Padilla, L. F., Munera Lopez, J., Liu, J., Brown, P. T., Murray, J. M. and Hu, K. (2023). The cortical microtubules of *Toxoplasma gondii* underlie the helicity of parasite movement. *J. Cell Sci.* 136, jcs261270. doi:10.1242/jcs.261270
- Torgerson, P. R. and Mastroiacovo, P. (2013). The global burden of congenital toxoplasmosis: a systematic review. *Bull. W.H.O* **91**, 501-508. doi:10.2471/BLT. 12.111732
- Tran, J. Q., De Leon, J. C., Li, C., Huynh, M. H., Beatty, W. and Morrissette, N. S. (2010). RNG1 is a late marker of the apical polar ring in *Toxoplasma gondii*. Cytoskeleton (Hoboken) 67, 586-598. doi:10.1002/cm.20469
- Voß, Y., Klaus, S., Guizetti, J. and Ganter, M. (2023). Plasmodium schizogony, a chronology of the parasite's cell cycle in the blood stage. PLoS Pathog. 19, e1011157. doi:10.1371/journal.ppat.1011157
- Wang, X., Qian, P., Cui, H., Yao, L. and Yuan, J. (2020). A protein palmitoylation cascade regulates microtubule cytoskeleton integrity in *Plasmodium*. *EMBO J*. 39, e104168. doi:10.15252/embj.2019104168
- Wang, X., Fu, Y., Beatty, W. L., Ma, M., Brown, A., Sibley, L. D. and Zhang, R. (2021). Cryo-EM structure of cortical microtubules from human parasite Toxoplasma gondii identifies their microtubule inner proteins. Nat. Commun. 12, 3065. doi:10.1038/s41467-021-23351-1